International Journal of Biology and Life Sciences
ISSN: 2957-9511 | Vol. 12, No. 3, 2025

ReliefF Feature Selection and a SSA-IRF Model for Continuous Blood Pressure Estimation from Electrocardiogram and Photoplethysmography Signals

Yunfei Ma, Yang Xiao, Wang Zhang

University of Shanghai for Science and Technology, Shanghai, China

Abstract: Blood pressure (BP) serves as a vital indicator of cardiovascular health; however, achieving accurate and continuous BP monitoring continues to present significant challenges. To enhance the performance of continuous BP estimation using electrocardiogram (ECG) and photoplethysmography (PPG) signals, this paper introduces a method that integrates the ReliefF feature weighting algorithm with a Sparrow Search Algorithm-optimized Iterative Random Forest (SSA-IRF) regression model. First, a comprehensive set of time-domain, frequency-domain, and time-frequency features is extracted from PPG and ECG signals. The ReliefF algorithm is then applied to select highly sensitive features strongly correlated with BP, thereby reducing redundancy and improving monitoring efficiency. Subsequently, a hybrid prediction model is developed by combining the Sparrow Search Algorithm (SSA) with an Iterative Random Forest (IRF) regression model to learn the mapping between the selected features and BP values. A novel fitness function is designed to balance prediction accuracy and consistency. Finally, ablation and comparative experiments were conducted using ECG and PPG signals from 200 subjects in the MIMIC-III database, validating the effectiveness and advancement of the proposed approach. Experimental results show that the method achieves a mean absolute error (MAE) of 2.73 mmHg and a standard deviation (STD) of 3.88 mmHg for systolic BP prediction, and an MAE of 1.62 mmHg with an STD of 2.31 mmHg for diastolic BP prediction. Its performance not only complies with the Association for the Advancement of Medical Instrumentation (AAMI) standards but also meets Grade A criteria according to the British Hypertension Society (BHS) protocol.

Keywords: Continuous Blood Pressure Monitoring; Photoplethysmography (PPG); Electrocardiogram (ECG); Feature Selection; ReliefF Algorithm; Sparrow Search Algorithm (SSA); Iterative Random Forest (IRF).

1. Introduction

Cardiovascular disorders associated with hypertension are widespread among the general population. In the initial phases, most individuals with hypertension do not display noticeable symptoms and often lack adequate awareness of their health status. Consequently, many fail to receive timely and standardized medical intervention, increasing the risk of serious complications such as cerebral thrombosis[1]. Hence, sustained blood pressure surveillance is crucial for hypertension prevention[2].

Existing blood pressure monitoring techniques are generally divided into direct and indirect approaches according to their underlying principles[3]. Direct measurement, performed by inserting a catheter into an artery, is considered the clinical gold standard for blood pressure evaluation. It is typically restricted to major surgical procedures or intensive care environments and is not feasible for prolonged monitoring. Indirect methods mainly encompass conventional cuff-based measurements and pulse arrival time (PAT) techniques[4]. Although cuff-based devices allow non-invasive readings at discrete time points, the necessity for periodic inflation limits them to intermittent operation. Moreover, this approach may yield inaccurate results, contributing to diagnostic errors such as masked or white-coat hypertension. The PAT method calculates the time interval between the ECG R-wave and the peak of the PPG signal. Research has shown that PAT is a promising parameter for enabling continuous blood pressure estimation, drawing substantial investigative attention[5]. Nevertheless, precise PAT determination depends on synchronous acquisition of ECG and PPG signals. The requirement for accurate placement of multiple sensors and the technical challenges of simultaneous signal capture constrain measurement reliability. Therefore, a new cuffless, non-invasive, and accurate blood pressure monitoring strategy is needed[6].

In 1992, Kenji Kira and Larry A. Rendell proposed a feature selection algorithm named ReliefF[7]. As a classic filter-based method, ReliefF offers notable benefits in blood pressure prediction compared to wrapper or embedded feature selection techniques: it delivers high computational efficiency due to its k-nearest neighbor evaluation mechanism, which reduces training overhead relative to approaches requiring repeated model training; it exhibits strong robustness by assessing feature relevance through weighted nearest-neighbor distances, thereby attenuating noise and redundant feature effects while accommodating mixed data types. Extended to regression tasks, ReliefF directly gauges the explanatory power of features for continuous blood pressure values.

Recently, studies employing machine learning models to estimate blood pressure from ECG and PPG signals have gained momentum. Investigators have concentrated on developing accurate and continuous blood pressure monitoring models by deriving multi-domain features from these signals[6]. This direction is motivated by two key factors: first, the growing use of wearable devices allows convenient and comfortable collection of ECG and PPG data, supplying a dependable foundation for blood pressure estimation; second, PPG waveforms reflect dynamic changes in intravascular blood volume and encompass rich cardiovascular information, while characteristic ECG

components—such as P, Q, R, S, and T waves—represent myocardial depolarization and repolarization, offering compelling physiological evidence for blood pressure assessment. Thambiraj et al. developed and compared feature models derived solely from PPG, solely from ECG, and from fused multi-signal data. Their findings revealed that the fused-signal model substantially outperformed single-signal versions[8]. Whereas individual signals provide limited information for blood pressure monitoring, multi-signal fusion yields complementary physiological insights, effectively improving estimation accuracy and reliability[9].

The reliability of blood pressure monitoring depends not only on appropriate feature selection but also on the predictive model's performance[12]. Deep learning, with its powerful data mining and automated feature learning abilities, has been extensively adopted across various fields[10]. Despite its strengths in automatic feature engineering, deep learning usually demands large-scale datasets for training, which can be difficult to obtain in clinical practice[11]. Additionally, the high computational cost and opaque "black-box" nature of many deep learning models limit interpretability. To balance performance and computational efficiency, machine learning has attracted growing interest in blood pressure monitoring due to its relatively lower data requirements. Among these methods, iterative random forests (IRF) reduce overfitting risk by building multiple independent random forests and aggregating their outputs[13],thereby improving generalization. However, IRF parameter tuning often relies on empirical adjustment, making it less adaptable to complex scenarios.

Advances in optimization algorithms have demonstrated the considerable potential of swarm intelligence methods for tuning machine learning parameters. The sparrow search algorithm (SSA), a recently proposed meta-heuristic technique, balances global exploration and local exploitation by simulating sparrow foraging and anti-predator behaviors [14]. It offers benefits such as fast convergence and minimal parameter requirements. Compared to the complex crossover and mutation operations of Genetic Algorithms (GA) or the single velocity update mechanism of Particle Swarm Optimization (PSO), SSA exhibits greater robustness in handling high-dimensional parameter spaces.

To overcome these limitations, this work introduces a continuous blood pressure monitoring approach based on ReliefF feature selection and a sparrow search algorithm-optimized iterative random forest (SSA-IRF) prediction model. The principal contributions are outlined below:

1. A continuous blood pressure monitoring framework integrating ReliefF feature selection and SSA-IRF regression models is proposed. ReliefF reduces feature redundancy by selecting highly discriminative attributes, while SSA optimizes IRF parameters to improve model generalization.

2. Comprehensive features are extracted from the time domain, frequency domain, and time-frequency domain of PPG and ECG signals to provide multidimensional physiological information for blood pressure monitoring. The ReliefF algorithm is employed to screen sensitive features highly correlated with blood pressure, addressing the issue where traditional filtering methods may overlook weakly correlated yet highly contributory features;

3. An SSA-IRF fusion prediction model is constructed. The global search capability of SSA optimizes key parameters of the IRF model, such as the number of trees and minimum leaf count, while the iterative ensemble mechanism of IRF reduces model variance, balancing monitoring accuracy and stability;

4. The effectiveness and superiority of the proposed method are verified through ablation studies and comparison with multiple alternatives. Experimental results confirm that it outperforms conventional filter-based feature selection combined with empirically tuned models, as well as other swarm intelligence optimization techniques, in continuous blood pressure monitoring tasks.

2. Materials and Methods

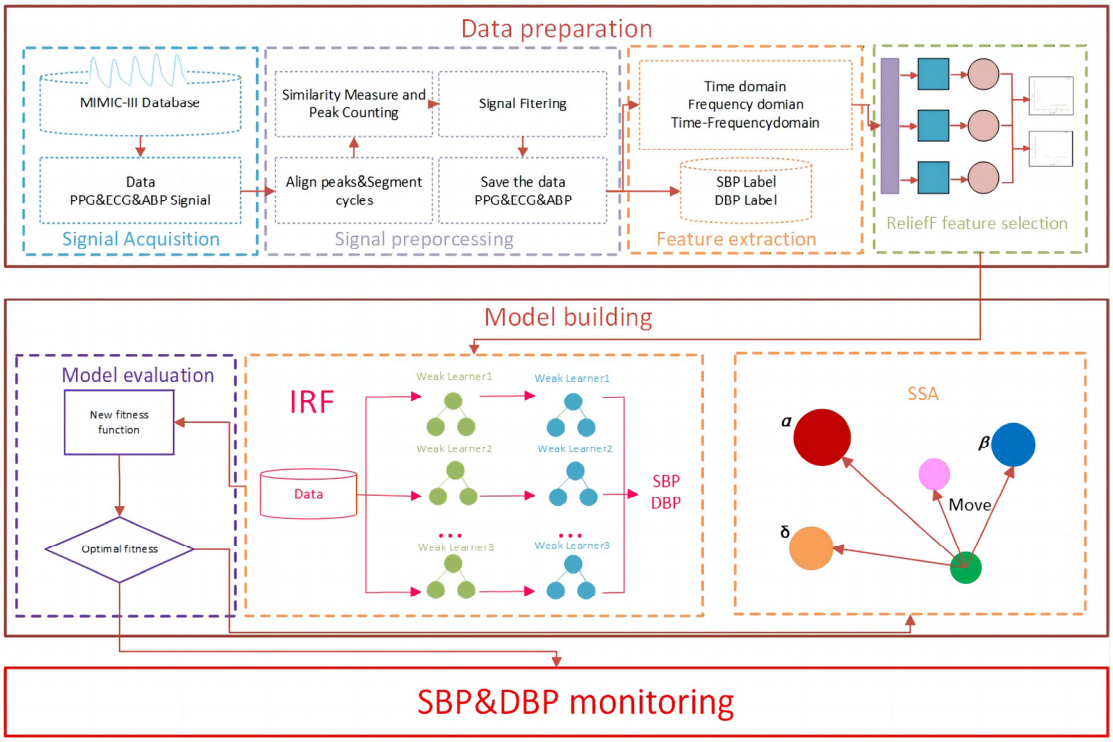


Fig 1. Framework of the proposed method for continuous blood pressure monitoring.

Fig. 1 outlines the workflow of the proposed continuous blood pressure (BP) monitoring system. The framework is organized into two main stages: data preparation and model development. The data preparation stage involves experimental data collection, raw signal preprocessing, feature extraction, and subsequent feature selection. In the model development phase, an initial predictive model is built using iterative random forests (IRF). Subsequently, the model parameters are fine-tuned via the Sparrow Search Algorithm (SSA), and the overall system performance is thoroughly evaluated.

2.1. Signal Acquisition

The experimental data utilized in this study were sourced from the MIMIC-III database[15], which contains raw digital waveforms recorded from approximately 60,000 intensive care unit (ICU) patients. These recordings consist of photoplethysmography (PPG), electrocardiography (ECG), and arterial blood pressure (ABP) signals. The ABP waveform was used as the reference standard for blood pressure estimation. Raw waveform data comprising PPG, ECG, and ABP were extracted from a subset of 200 patients, with a gender distribution of 38% female and 62% male.

2.1.1. Data Pre-processing

In practical applications, signal preprocessing represents a crucial and effective stage for removing noise contamination, thereby improving the monitoring accuracy of subsequent blood pressure prediction models. The outlier removal framework is illustrated in **Fig 2**.

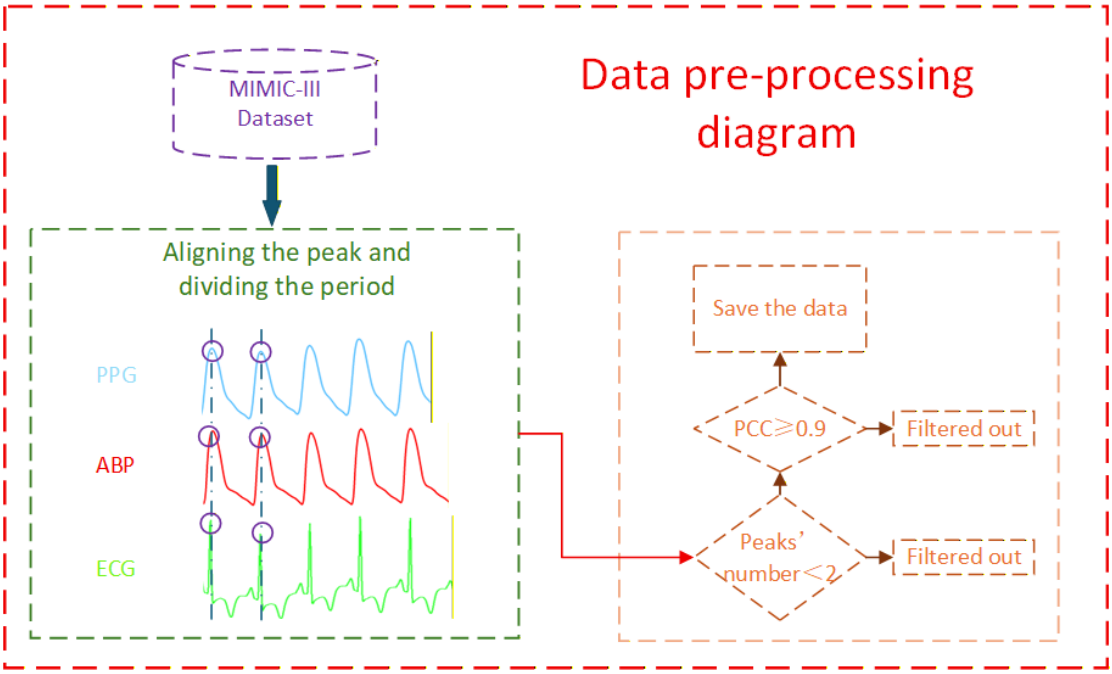


Fig 2. Data pre-processing diagram.

Initially, photoplethysmography (PPG), electrocardiography (ECG), and arterial blood pressure (ABP) signals were temporally aligned using waveform matching techniques and segmented into individual cycles. Qualitative analysis revealed negligible contamination in the ECG signals across the dataset; therefore, feature extraction was confined to cycles derived from PPG and ABP signals. The Pearson correlation coefficient (PCC), a robust indicator of linear association between two variables, was utilized for signal selection. The PCC is defined by Eq.1:

$$PCC = r = \frac{n\sum_{i=1}^{n} x_i y_i - \left(\sum_{i=1}^{n} x_i\right)\left(\sum_{i=1}^{n} y_i\right)}{\sqrt{\left[n\sum_{i=1}^{n} x_i^2 - \left(\sum_{i=1}^{n} x_i\right)^2\right]\cdot}} \quad (1)$$

where N is the sample size, Xi and Yi denote two independent samples, the mean of X is $\frac{1}{N}\sum_{i=1}^{N} x_I$, and similarly, the mean of Y is $\frac{1}{N}\sum_{i=1}^{N} y_I$.

During the outlier exclusion phase, only signal cycles exhibiting a PCC greater than 0.9 were retained. Furthermore, each cycle was constrained to contain no more than a single peak. For the purposes of this experiment, the initial 10,000 data points were selected to constitute the dataset. A representative example of preprocessed multimodal signals—PPG, ECG, and ABP—obtained from one patient is illustrated in **Fig 3**.

2.2. Feature Extraction and Selection

Numerous investigations have demonstrated the utility of multi-domain features derived from electrocardiogram (ECG) and photoplethysmogram (PPG) signals in blood pressure estimation[8]. Evidence suggests that expanding the repertoire of discriminative features can improve the predictive performance of computational models. Accordingly, to furnish a comprehensive feature set for blood pressure monitoring, this study extracts temporal, spectral, and time-frequency attributes from preprocessed PPG and ECG recordings.

In the time domain, the PPG signal yields metrics such as pulse widths at different amplitude fractions, pulse area, systolic and diastolic time intervals, peak-to-peak duration, and characteristics of its derivative waveform[16]. Simultaneously, amplitude-based and interval-based parameters are derived from the ECG. Conversion of temporal signals into the frequency domain is achieved through Fast Fourier Transform (FFT), thereby capturing oscillatory patterns across the frequency spectrum. Additionally, time-frequency representations are utilized to

extract entropy-based descriptors, including wavelet energy entropy, wavelet scale entropy, and wavelet singular entropy.

All extracted features are shown in the Table 1.

Table 1. List of features

Number	Symbol	Definition
1	tpi-t1	Diastolic Width
2	t1	Time interval from the PPG waveform onset to the systolic peak
3	tpi-t2	Endpoint Z of the PPG waveform
4	X	Amplitude of the PPG systolic peak
5	A1	Area under the PPG systolic phase
6	A2	Area under the PPG diastolic phase
7	A2/A1	Ratio of diastolic area to systolic area
8	DW10	Waveform width at 10% of diastolic amplitude
9	DW25	Waveform width at 25% of diastolic amplitude
10	DW33	Waveform width at 33% of diastolic amplitude
11	DW50	Waveform width at 50% of diastolic amplitude
12	DW66	Waveform width at 66% of diastolic amplitude
13	DW75	Waveform width at 75% of diastolic amplitude
14	SW75	Waveform width at 75% of systolic amplitude
15	DW75/SW75	Ratio of waveform width at 75% diastolic amplitude to waveform width at 75% systolic amplitude
16	SW10/tpi-t1	Ratio of waveform width at 10% systolic amplitude to diastolic width
17	SW25/tpi-t1	Ratio of waveform width at 25% systolic amplitude to diastolic width
18	SW33/tpi-t1	Ratio of waveform width at 33% systolic amplitude to diastolic width
19	SW50/tpi-t1	Ratio of waveform width at 50% systolic amplitude to diastolic width
20	SW66/tpi-t1	Ratio of waveform width at 66% systolic amplitude to diastolic width
21	SW75/tpi-t1	Ratio of waveform width at 75% systolic amplitude to diastolic width
22	a1	Amplitude of point a1 in the first derivative of the PPG signal
23	t_a1	Time interval from the first derivative waveform onset to point a1
24	b1	Amplitude of point b1 in the first derivative of the PPG signal
25	t_b1	Time interval from the first derivative waveform onset to point b1
26	b1/a1	Ratio of amplitude at point b1 to amplitude at point a1 in the first derivative
27	a2	Amplitude of point a2 in the second derivative of the PPG signal
28	b2	Amplitude of point b2 in the second derivative of the PPG signal
29	t_b2	Time interval from the second derivative waveform onset to point b2
30	b2/a2	Ratio of amplitude at point b2 to amplitude at point a2 in the second derivative
31	T_QR	Time interval from point R to point Q in the ECG signal
32	T_RS	Time interval from point R to point S in the ECG signal
33	T_RR	Time interval from point R to point R in the ECG signal (R-R interval)
34	T_PR	Time interval from point R to point P in the ECG signal
35	T_QT	Time interval from point T to point Q in the ECG signal (Q-T interval)
36	T_ST	Time interval from point T to point S in the ECG signal (S-T interval)
37	H_R	Amplitude of point R in the ECG signal
38	H_Q	Amplitude of point Q in the ECG signal
39	H_S	Amplitude of point S in the ECG signal
40	H_P	Amplitude of point P in the ECG signal
41	H_T	Amplitude of point T in the ECG signal
42-43	Peak_1	Amplitude of the first peak obtained from the FFT of PPG and ECG signals
44	Peak_3	Amplitude of the third peak obtained from the FFT of the ECG signal
45-46	A0-2	Area under the curve from the FFT onset to the second peak for PPG and ECG signals
47	A0-1/A0-2	Ratio of area A0-1 to area A0-2
48	E1	Wavelet Scale Entropy of the 8 sub-bands for the ECG signal
49	WSE	Wavelet Singularity Entropy for PPG and ECG signals

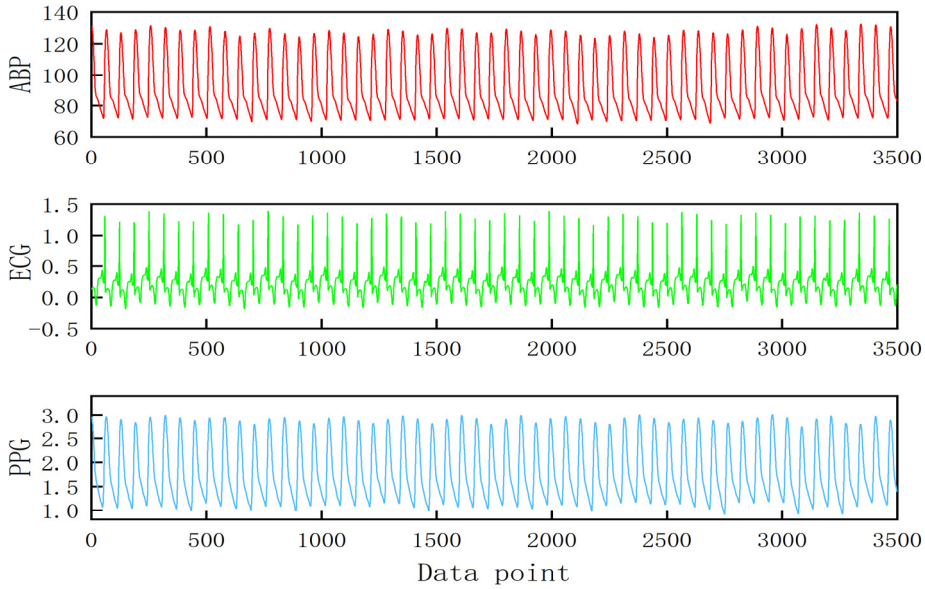


Fig 3. A patient's ABP, ECG, PPG signal going through data pre-processing

2.3. ReliefF-selected Features

To mitigate the risk of overfitting and enhance computational efficiency, feature selection was performed on the extracted time-domain, frequency-domain, and time-frequency-domain features. This study employed the ReliefF algorithm to quantitatively assess the relevance of each feature for BP prediction[12]. The core mechanism of ReliefF involves iteratively estimating feature weights based on a feature's ability to distinguish between nearest neighbor instances. For a given feature [F], its weight W[F] is updated as Eq 2:

$$W[F] = W[F] - \frac{\sum_{k=1}^{K} diff(F,R,H_k)}{K \cdot m} + \frac{\sum_{C \neq class(R)} \left[\frac{P(C)}{1-P(class(R))} \sum_{k=1}^{K} diff(F,R,M_k(C))\right]}{K \cdot m} \quad (2)$$

where:R is a randomly selected instance,$H_k$denotes the k-th nearest hit, M_k©denotes the k-th nearest miss,K is the number of nearest neighbors,m is the number of sampling iterations, P© is the prior probability of class C,$diff(F, I_1, I_2)$ computes the difference in the values of feature Fbetween two instances $I_1$and I_2.

Features were then ranked in descending order of their final weights W[F]. These sorted features were sequentially incorporated into a Gradient Boosting Regression model. The optimal feature subset size was determined by identifying the point where both Mean Absolute Error (MAE) and Mean Squared Error (MSE) were minimized. The analysis revealed that the top 21 features for SBP and the top 20 features for DBP yielded the lowest prediction errors. The final selected features are presented in Table 2.

Table 2. List of ReliefF-selected features

	DBP	SBP
Number	31,4,30,5,28,2,29,25,27,26,47,42,43,38,22,35,49,23,45,46,48	31,4,30,5,28,2,29,25,27,26,47,42,43,38,22,35,49,23,45,46

2.4. IRF-Based Initial Model

Iterative Random Forest Regression models represent an enhancement over classical Random Forest Regression[13] . Their core principle involves constructing a series of interconnected Random Forests through multiple iterative rounds, progressively improving feature selection and model prediction accuracy to ultimately form a more robust ensemble model. This approach is particularly well-suited for regression tasks requiring the capture of complex feature interactions, such as blood pressure prediction. Assume the training dataset contains N samples, where x_I represents the input feature vector and y_I denotes the corresponding actual blood pressure value. IRF begins with an initial random forest mode $IRF^{(0)}(x)$, composed of K regression trees, whose ensemble prediction is Eq.3:

$$y_i^{(0)} = \frac{1}{K} \sum_{k=1}^{K} T_k^{(0)}(x_i) \quad (3)$$

Where $T_k^{(0)}$ denotes the k-th regression tree in the initial forest. The core of the iterative process lies in utilizing feedback from the previous model to guide subsequent forest training. For the m-th iteration (m=1,2,...,m):

Based on the feature importance metric computed by the previous forest RF(m-1), update the weight $w_j^{(m)}$ for each feature in Eq.4:

$$w_j^{(m)} = g\left(Importance_j^{(m-1)}, w_j^{(m-1)}\right) \quad (4)$$

Whereg(·) is a predefined update function that takes the previous round's importance scores $Importance_j^{(m-1)}$ and previous weights $w_j^{(m-1)}$ as inputs. The updated weights reflect the current assessment of feature importance.

Train a new random forest $RF^{(m)}(x)$ using the updated feature weights $w^{(m)}$. During forest construction, the probability of a feature being sampled is proportional to its weight $w_j^{(m)}$ in Eq.5:

$$P(\text{select feature } j) \propto w_j^{(m)} \tag{5}$$

The newly trained forest $RF^{(m)}$ is added to the ensemble model. As shown in **Fig.4**, the ensemble prediction after the m-th iteration is the simple average of all existing forest predictions in Eq.6:

$$y_i^{(m)} = \frac{1}{m+1} \sum_{l=0}^{m} R F^{(l)}(x_i) \tag{6}$$

To prevent overfitting and enhance the generalization of the model to new blood pressure data, the number of iterations *M* serves as a key regularization parameter. The iterative process is typically stopped once the performance on an independent validation set stabilizes—or when a predetermined upper limit of iterations is attained. A value of *M* that is too small can restrict the model's ability to capture relevant feature interactions, while an excessively high M may produce overly intricate models that adapt to noise in the training set.

Furthermore, hyperparameters within each base random forest—including maximum tree depth, minimum samples per leaf, the number of trees *K*, and the precise formulation of the feature weight update $(\cdot)$—demand careful adjustment using methods such as cross-validation. This optimization should be informed by the particular characteristics of the blood pressure dataset to achieve an optimal trade-off between predictive accuracy and computational cost. Within this iterative weighted feature selection framework, IRF can more consistently detect and utilize higher-order feature combinations that are strongly linked to changes in blood pressure.

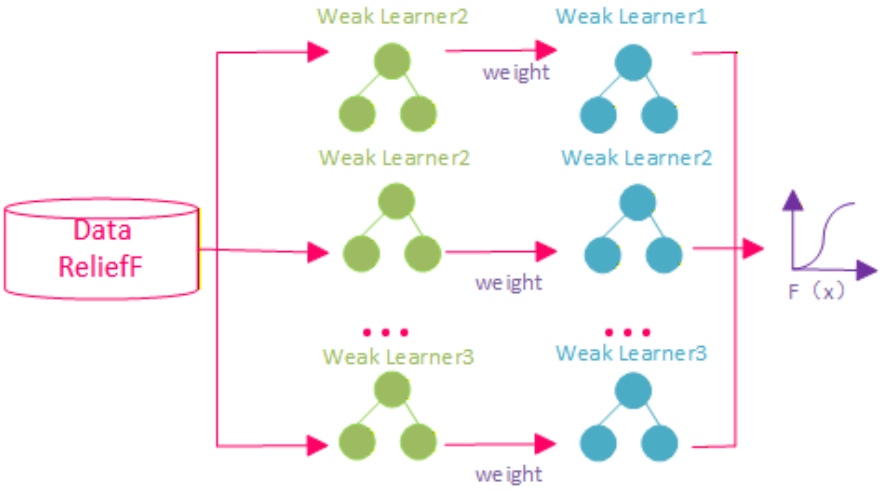


Fig.4. Iterative random forest algorithm

2.5. Sparrow Search Optimization Algorithm

The Sparrow Search Algorithm (SSA) was proposed by Xue Jiankai in 2020[14]. It simulates the unique producer-scrounger mechanism and the vigilant anti-predation behavior observed in sparrow flocks during foraging. During foraging, individuals within the sparrow population are abstracted into three roles: discoverers, followers, and sentinels. discoverers are responsible for locating areas rich in food resources and guiding the foraging direction for the entire population. Followers utilize information from the producers to forage in their vicinity. Sentinels continuously monitor the environment; upon detecting danger, they issue alarm signals and guide the flock to safer areas, thereby avoiding predation risks, as shown in **Fig 5**. SSA achieves optimization search by mathematically modeling the cooperative and competitive mechanisms among these three roles. Its primary position update formula is as follows:

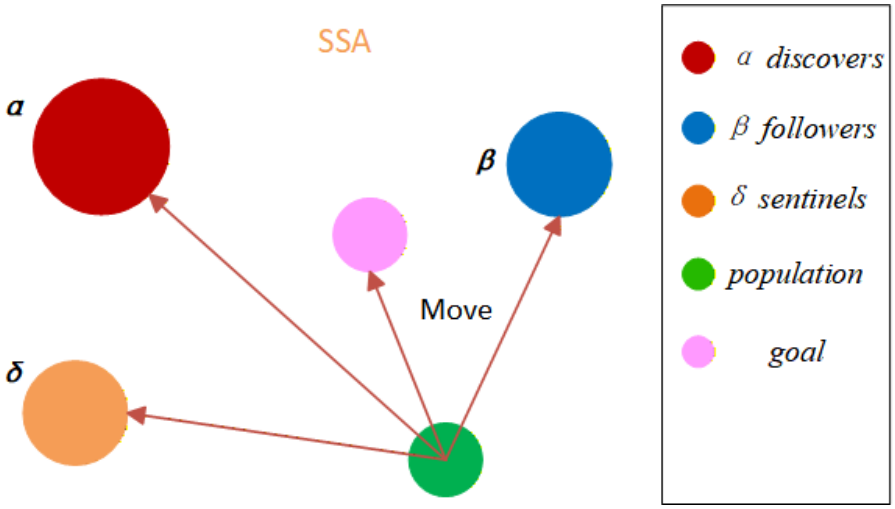


Fig 5. Position update in SSA.

Explorer Position Update in Eq.7:

$$X_{i,j}^{t+1} = \begin{cases} X_{i,j}^{t} \cdot \exp\left(-\frac{i}{\alpha \cdot T_{max}}\right), & R_2 < ST \\ X_{i,j}^{t} + Q \cdot L, & R_2 \geq ST \end{cases} \quad (7)$$

Where T_{max} denotes the maximum iteration count, α is a constant, $R_2 \in [0,1]$ represents the early warning threshold, $ST \in [0.5,1]$ denotes the safety threshold, Q is a normally distributed random number, and L is the unit row vector.

Follower Position Update in Eq.8:

$$X_{i,j}^{t+1} = \begin{cases} Q \cdot \exp\left(\frac{X_{worst}^{t} - X_{i,j}^{t}}{i^2}\right), & i > \frac{n}{2} \\ X_{P}^{t+1} + \left|X_{i,j}^{t} - X_{P}^{t+1}\right| \cdot A^{+} \cdot L, & i \leq \frac{n}{2} \end{cases} \quad (8)$$

Where X_p is the current optimal position, X_{worst} is the worst position, and A is a matrix with elements ±1.3

Patrol position update in Eq.9:

$$X_{i,j}^{t+1} = X_{best}^{t} + \beta \cdot \left|X_{i,j}^{t} - X_{best}^{t}\right| \cdot r \quad (9)$$

Where X_{best} is the global optimal position, β is the step size control parameter, and r is a random vector.

The algorithm balances exploration and exploitation through the synergistic mechanism of these three components. Literature studies indicate it demonstrates greater competitiveness than other algorithms in terms of convergence speed and accuracy **Fig 6** clearly show the whole workflow of SSA.

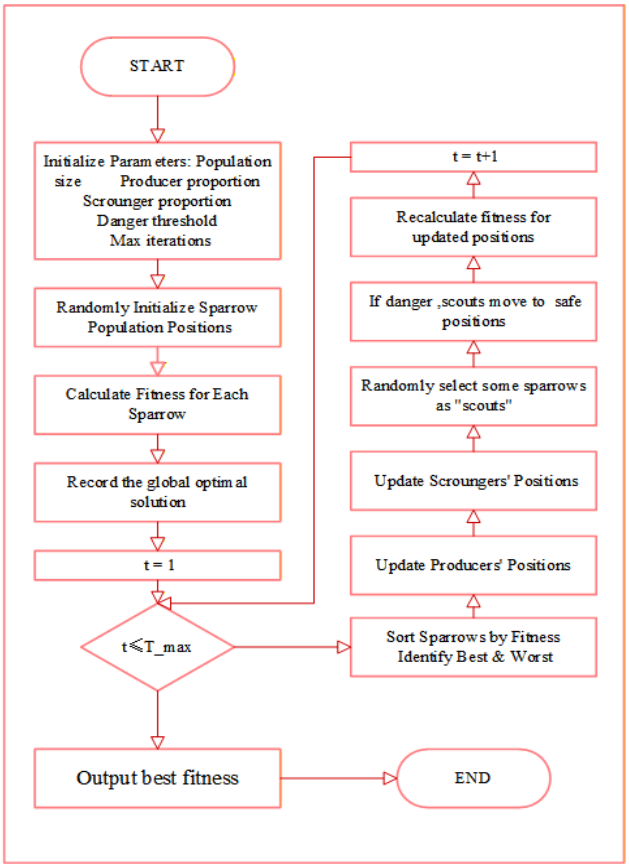


Fig 6. Workflow diagram of the SSA algorithm.

2.6. Performance Evaluation Metric

This study employs four metrics to comprehensively assess the predictive capability of the proposed ReliefF-SSA-IRF model.

1) Mean absolute error (MAE), and the expression is as follows:

$$MAE = \frac{1}{n}\sum_{i=1}^{n} |y_i - \hat{y}_i| \quad (10)$$

2) Mean square error (MSE), and the expression is as follows:

$$MSE = \frac{1}{n}\sum_{i=1}^{n} (y_i - \hat{y}_i)^2 \quad (11)$$

3) Standard deviation (STD), and the expression is as follows:

$$STD = \sqrt{\frac{1}{n-1}\sum_{i=1}^{n} (x_i - \bar{x})^2} \quad (12)$$

4) Pearson correlation coefficient (PCC), and the expression is as follows:

$$PCC = \frac{\sum_{i=1}^{n} (x_i - \bar{x})(y_i - \bar{y})}{\sqrt{\sum_{i=1}^{n} (x_i - \bar{x})^2 \sum_{i=1}^{n} (y_i - \bar{y})^2}} \quad (13)$$

3. Results and Analysis

3.1. Analysis of Feature Selection

In this study, five advanced feature selection techniques—Kernel Principal Component Analysis (KPCA), Maximum Relevance Minimum Redundancy (MRMR), Locally Linear Embedding (LLE), Mean Impact Value (MIV), and Random Forest-based feature selection (RFFS)—were employed to assess the comparative performance of the ReliefF-based feature selection strategy.

All feature selection procedures were implemented within the framework of two robust predictive models: a Bayesian Regularized Artificial Neural Network (BRANN) and an Iterative Random Forest (IRF). As illustrated in **Fig 7** and **Fig 8**, which summarize and compare the Mean Absolute Error (MAE) and Standard Deviation (STD) for systolic and diastolic blood pressure predictions across the different model configurations, the ReliefF-driven feature selection approach consistently demonstrated superior performance relative to other methods under both predictive modeling paradigms. Consequently, the proposed feature selection technique proves effective in identifying features with strong relevance to blood pressure, thereby contributing to enhanced predictive accuracy in BP monitoring methodologies.

3.2. Analysis of Regression Models

Subsequently, we compared the IRF model with seven state-of-the-art regression models: Gaussian Process Regression (GPR), Random Forest (RFFS), Gradient Boosted Regression Trees (GBRT), Bayesian Regularized Artificial Neural Networks (BRANN), Least Squares Support Vector Regression (LSSVR), Multiple Linear Regression (MLR), and Decision Tree Regression (DTR). As illustrated in **Fig 9**and **Fig 10**, the IRF-based model exhibited significantly lower MAE and STD values than the other regression models for both systolic and diastolic blood pressure predictions. These results demonstrate that the proposed model achieves high predictive accuracy for continuous blood pressure monitoring.

3.3. Ablation Studies and Results Analysis

This study performs ablation experiments on a consistent dataset to assess the contribution of individual components within the proposed ReliefF-SSA-IRF framework for continuous blood pressure monitoring. The framework combines three core modules: ReliefF-based feature selection, an IRF (Improved Random Forest) preliminary prediction model, and SSA (Sparrow Search Algorithm)-driven

parameter optimization. Predictive performance across different ablated configurations is evaluated using correlation analysis and error distribution histograms. Correlation analysis, which reflects the degree of agreement between predicted and reference blood pressure values, serves as a key indicator of model accuracy.

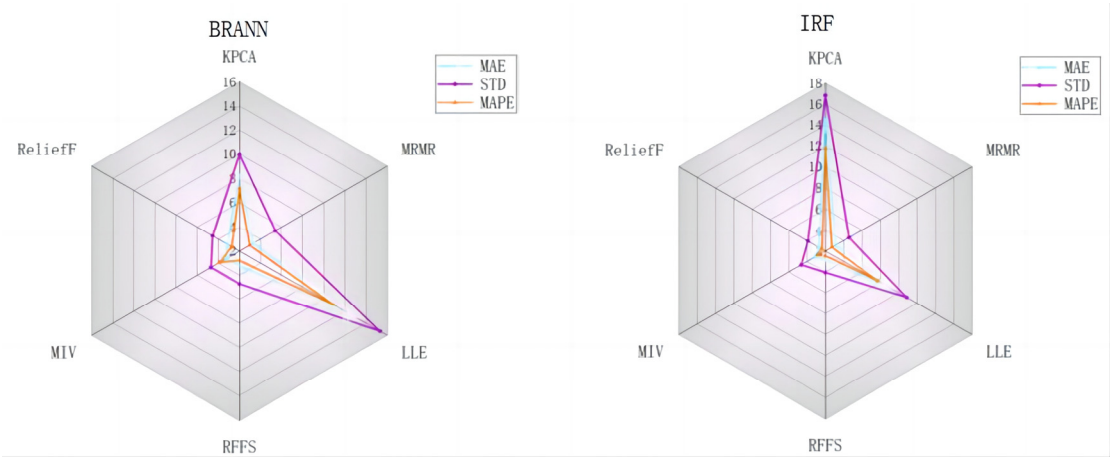


Fig 7. Comparison of feature selection methods for predicting SBP under different models.

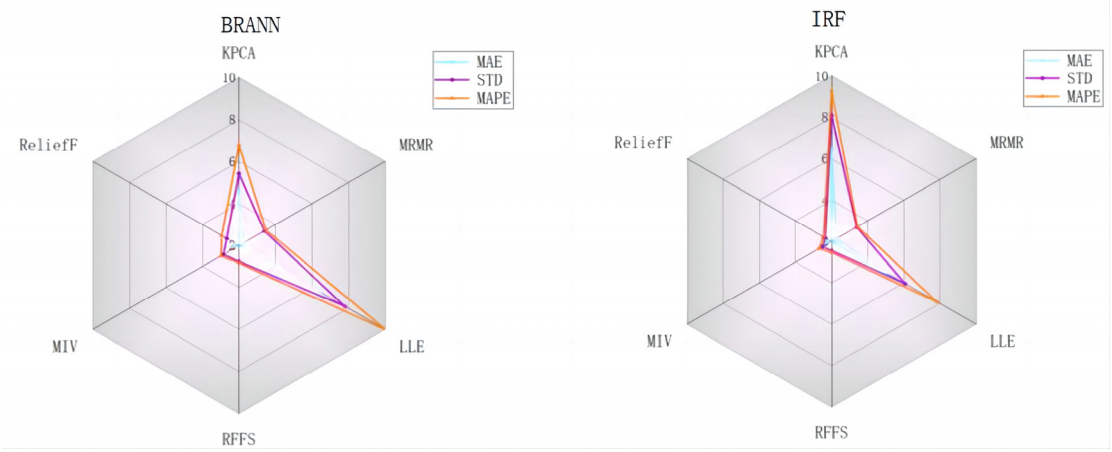


Fig 8. Comparison of feature selection methods for predicting DBP under different models.

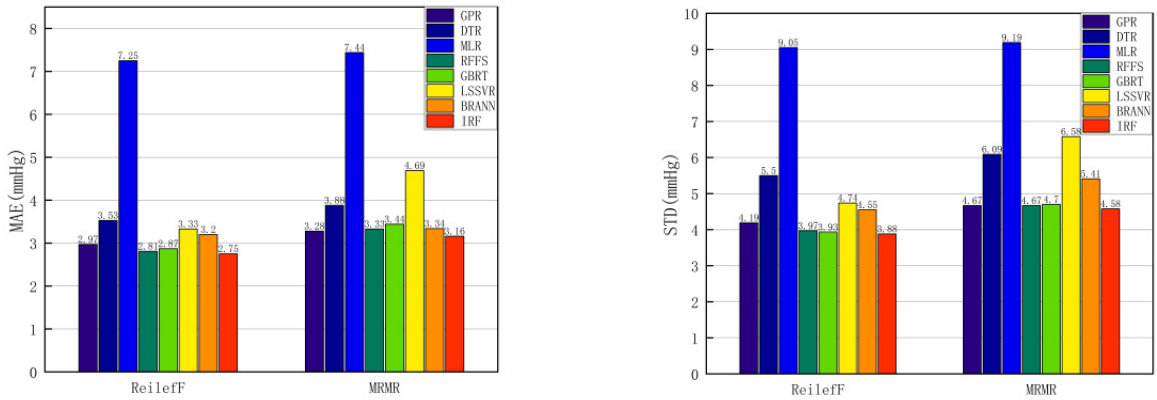


Fig 9. Comparisons of MAE and STD of the predicted SBP under different feature selection methods.

As shown in **Fig 11** and **Fig 12**,the ReliefF-IRF model (without SSA optimization) achieves correlation coefficients similar to those of the standalone IRF model. This indicates that the ReliefF feature selection module effectively reduces input dimensionality while preserving predictive fidelity, thereby enhancing the training efficiency of the IRF model. Furthermore, the complete ReliefF-SSA-IRF framework yields the strongest correlations, with coefficients reaching 0.92 for systolic blood pressure (SBP) and 0.90 for diastolic blood pressure (DBP). These results demonstrate that the SSA algorithm effectively identifies near-optimal parameters for the Gradient Boosting Regression Tree (GBRT) model. Overall, the integrated ReliefF-SSA-IRF framework surpasses its ablated counterparts, leading to significantly improved accuracy in blood pressure estimation.

In addition, **Fig 13** and **Fig 14** display the error histograms of SBP and DBP predictions for each ablation model. It can be observed that the prediction errors of the ReliefF-SSA-IRF

model for both SBP and DBP are closer to zero compared to those of the GBRT and ReliefF-IRF models.

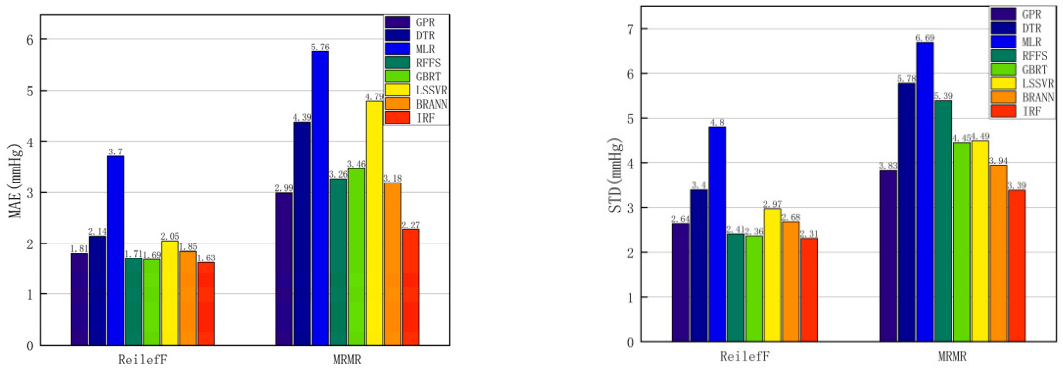


Fig 10. Comparisons of MAE and STD of the predicted DBP under different feature selection methods.

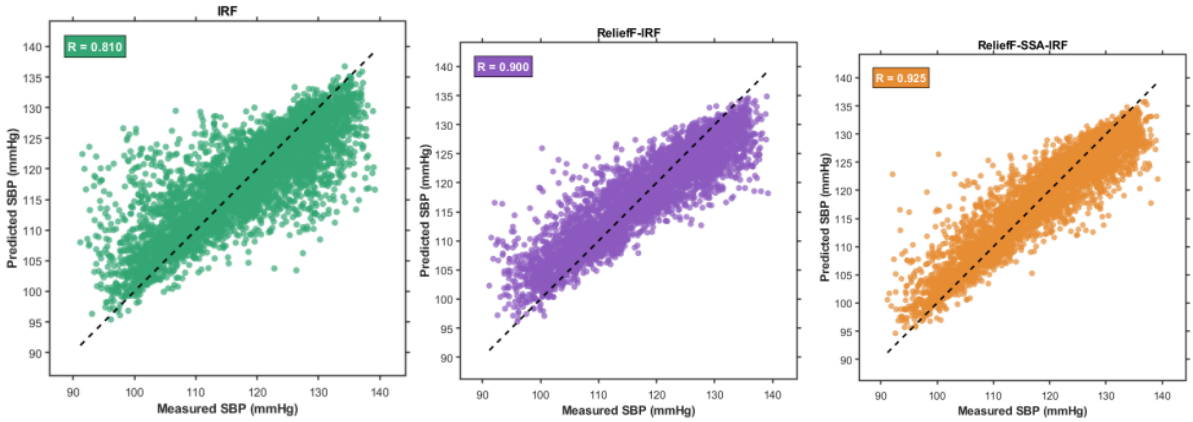


Fig 11. Correlation analysis between the predicted and actual SBP under different ablation models.

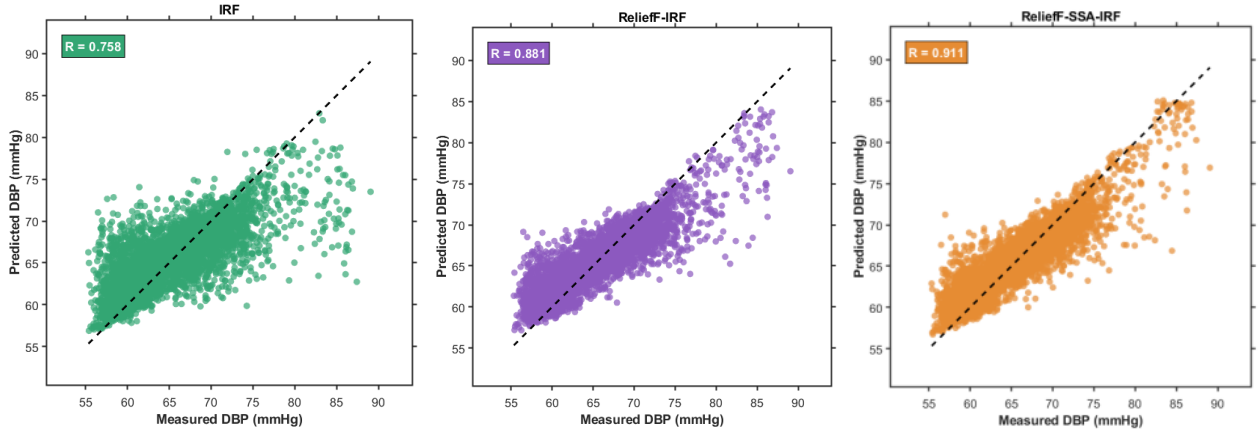


Fig 12. Correlation analysis between the predicted and actual DBP under different ablation models

To facilitate a direct comparison of error distributions across models, Figures 3.25 and 3.26 also present the percentage of monitored samples with BP errors within ±5 mmHg relative to the total number of BP samples. The results show that for the ReliefF-SSA-IRF model, 82.91% of SBP predictions and 96.30% of DBP predictions fall within the ±5 mmHg error range. These proportions are substantially higher than those of the other ablation models, providing further evidence that the proposed model achieves more accurate blood pressure monitoring.

Fig 15 presents Bland-Altman plots for the model's BP predictions. For DBP, 95.17% of the samples fall within the limits of agreement, while for SBP, 94.91% of samples remain within these limits. Overall, these findings indicate that the BP values predicted by the ReliefF-SSA-IRF model are in strong agreement with the actual measured values.

3.4. International Standard Validation

In this section, we validate the model's experimental results against two international standards: the British Hypertension Society (BHS) and the American Association of Medical Instrumentation (AAMI) [17], comprehensively verifying the effectiveness of our proposed model.

The BHS standard specifies cumulative absolute errors between predicted and true values in the total sample must be less than 5 mmHg, 10 mmHg, and 15 mmHg, respectively, classifying blood pressure prediction models into three grades: A, B, or C. Devices meeting BHS grading criteria at Grade A

or B are deemed suitable for clinical use. As shown in Table 3 our proposed method meets Grade A requirements for predicting both SBP and DBP.

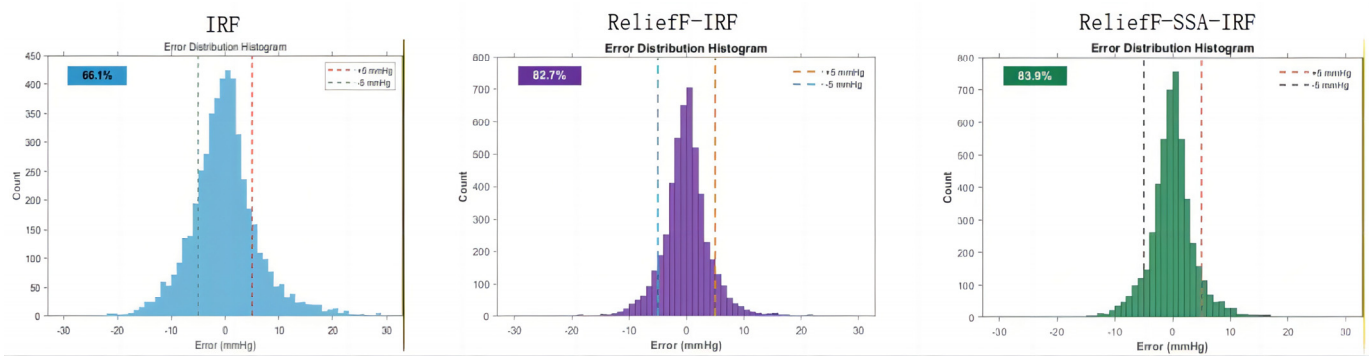


Fig 13. Error histogram of the predicted SBP under different ablation models.

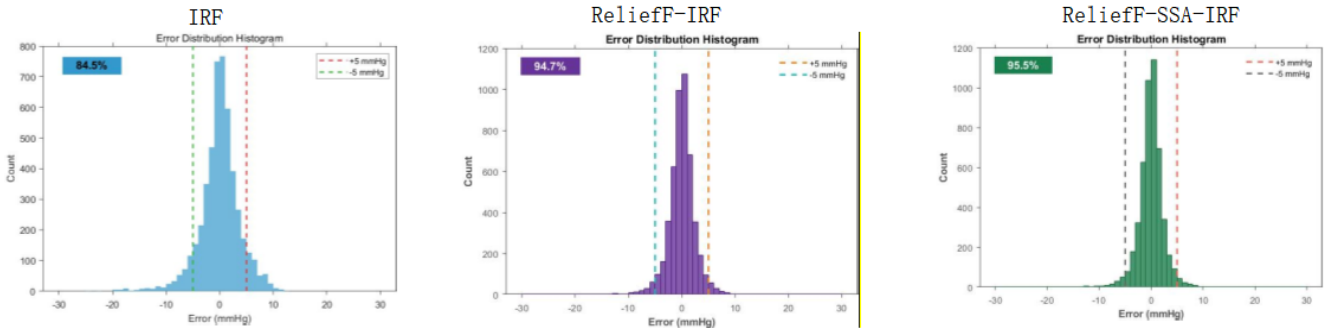


Fig 14. Error histogram of the predicted DBP under different ablation models.

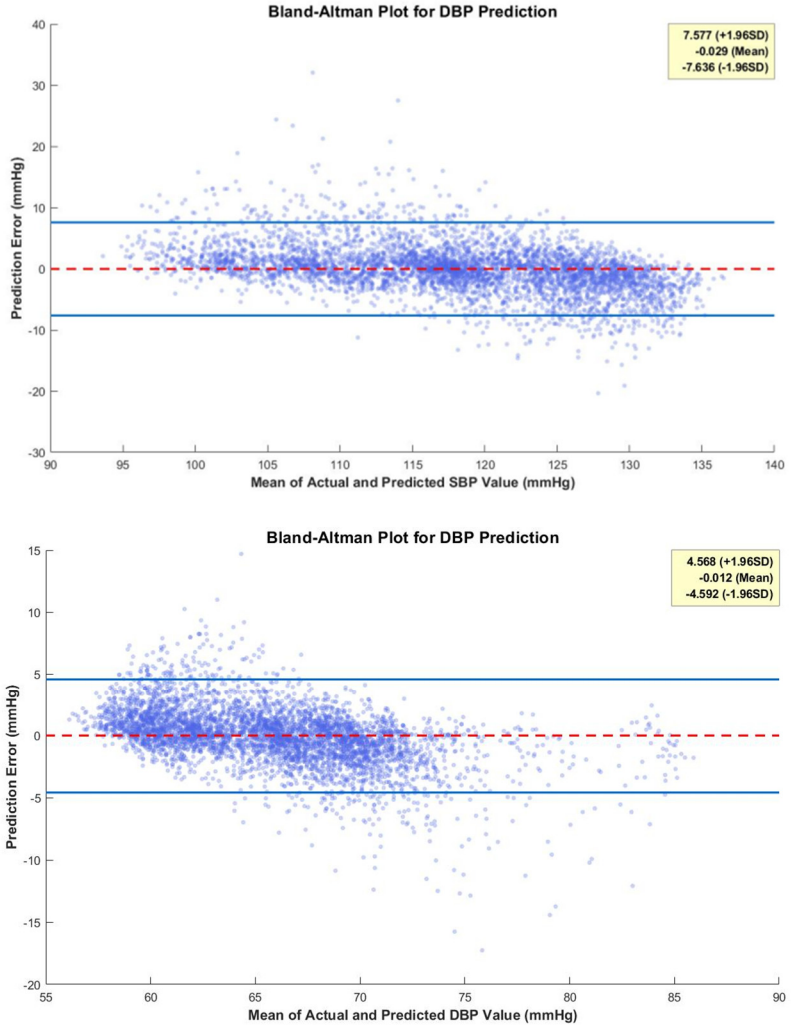


Fig 15. Bland-Altman plots of the predicted SBP (a) and DBP (b) using the ReliefF-SSA-IRF model.

Table 3. Performance Evaluation of the Proposed Method Using BHS Standards

BP	Error (%)			Grade
	<=5mmHg	<=10mmHg	<=15mmHg	
	60%50%40%	85%75%65%	95%90%85%	A/B/C
SBP	83.90%	97.57%	98.61%	A
DBP	95.30%	99.67%	99.92%	A

The AAMI standard specifies MAE <=5 mmHg and STD <= 8 mmHg for predicted blood pressure. As shown in Table 4, the MAE and STD for systolic pressure predicted by this method were 2.73 and 3.88 mmHg, respectively, both meeting the standard requirements. The MAE and STD for diastolic pressure predicted by this method were 1.621 and 2.31 mmHg, respectively, both significantly outperforming the standard. Based on the above results, this method demonstrates good accuracy and reliability in continuous BP monitoring.

Table 4. Performance Evaluation of the Method Using AAMI Standards

BP	MAE	STD	Grade
	≤5.00	≤8.00	
SBP	2.73	3.88	Pass
DBP	1.62	2.31	Pass

4. Conclusion

This study introduces a method for continuous blood pressure (BP) monitoring that integrates ReliefF-based feature selection with an SSA-IRF prediction model, thereby enhancing the performance of BP estimation using photoplethysmography (PPG) and electrocardiogram (ECG) signals. Following signal preprocessing, a comprehensive set of multi-domain features is derived from the PPG and ECG waveforms. The ReliefF algorithm is subsequently applied to identify the most informative features strongly associated with BP variations. A hybrid predictive model is then constructed by combining singular spectrum analysis (SSA) with an improved random forest (IRF) algorithm, utilizing a specifically formulated fitness function for optimization. The proposed framework is rigorously evaluated through ablation studies and comparative experiments, confirming its effectiveness and superiority. Results demonstrate that the ReliefF-SSA-IRF model outperforms existing state-of-the-art approaches in prediction accuracy. The system meets the Association for the Advancement of Medical Instrumentation (AAMI) requirements and attains Grade “A” according to the British Hypertension Society (BHS) protocol. Consequently, this work advances the practical application of PPG and ECG signals in BP monitoring, offering a promising direction for achieving cost-effective, accurate, and cuffless continuous BP measurement.

References

[1] Mills, K. T., Stefanescu, A., & He, J. (2020). The global epidemiology of hypertension. NATURE REVIEWS NEPHROLOGY, 16(4), 223-237. https://doi.org/10. 1038/s 41581- 019-0244-2.

[2] Schutte, A. E., Kollias, A., & Stergiou, G. S. (2022). Blood pressure and its variability: classic and novel measurement techniques. NATURE REVIEWS CARDIOLOGY, 19(10), 643-654. https://doi.org/10.1038/s41569-022-00690-0.

[3] Mukkamala, R., Stergiou, G. S., & Avolio, A. P. (2022). Cuffless Blood Pressure Measurement. ANNUAL REVIEW OF BIOMEDICAL ENGINEERING, 24, 203-230. https:// doi. org/ 10.1146/annurev-bioeng-110220-014644.

[4] Poon, C. C. Y., Zhang, Y. T., & Ieee. (2005). Cuff-less and noninvasive measurements of arterial blood pressure by pulse transit time 2005 27TH ANNUAL INTERNATIONAL CONFERENCE OF THE IEEE ENGINEERING IN MEDICINE AND BIOLOGY SOCIETY, VOLS 1-7.

[5] Kachuee, M., Kiani, M. M., Mohammadzade, H., & Shabany, M. (2017). Cuffless Blood Pressure Estimation Algorithms for Continuous Health-Care Monitoring. IEEE TRANSACTIONS ON BIOMEDICAL ENGINEERING, 64(4), 859-869. https:// doi. org/10.1109/TBME.2016.2580904.

[6] Mancia, G., & Grassi, G. (2014). The Autonomic Nervous System and Hypertension. CIRCULATION RESEARCH, 114 (11), 1804-1814. https://doi.org/10. 1161/ CIRCRESAHA. 114. 302524.

[7] Kira, K., & Rendell, L. A. (1992). The feature selection problem: Traditional methods and a new algorithm. In *Proceedings of the Tenth National Conference on Artificial Intelligence (AAAI-92)* (pp. 129-134).

[8] Thambiraj, G., Gandhi, U., Mangalanathan, U., Jose, V. J. M., & Anand, M. (2020). Investigation on the effect of Womersley number, ECG and PPG features for cuff less blood pressure estimation using machine learning. Biomedical Signal Processing and Control, 60, 101942. https://doi.org/https:// doi. org/ 10.1016/j.bspc.2020.101942.

[9] Song, M. S., & Lee, S. B. (2026). Interpretable machine learning for hypertension detection using photoplethysmography (PPG) signals and their derivatives. Biomedical Signal Processing and Control, 113, Article 109194. https://doi.org/10.1016/j.bspc.2025.109194.

[10] Slapnicar, G., Mlakar, N., & Lustrek, M. (2019). Blood Pressure Estimation from Photoplethysmogram Using a Spectro-Temporal Deep Neural Network. SENSORS, 19(15), Article 3420. https://doi.org/10.3390/s19153420.

[11] Li, Y. H., Harfiya, L. N., Purwandari, K., & Lin, Y. D. (2020). Real-Time Cuffless Continuous Blood Pressure Estimation Using Deep Learning Model. SENSORS, 20(19), Article 5606. https:// doi.org/10.3390/s20195606.

[12] Flórez-López, R. (2002). Reviewing RELIEF and its extensions:: A new approach for estimating attributes considering high-correlated features 2002 IEEE INTERNATIONAL CONFERENCE ON DATA MINING, PROCEEDINGS.

[13] Basu, S., Kumbier, K., Brown, J. B., & Yu, B. (2018). Iterative random forests to discover predictive and stable high-order interactions. PROCEEDINGS OF THE NATIONAL ACADEMY OF SCIENCES OF THE UNITED STATES OF AMERICA, 115(8), 1943-1948. https://doi.org/ 10.1073/ pnas. 1711236115.

[14] Xue, J. K., & Shen, B. (2020). A novel swarm intelligence optimization approach: sparrow search algorithm. SYSTEMS SCIENCE & CONTROL ENGINEERING, 8(1), 22-34. https:// doi.org/10.1080/21642583.2019.1708830.

[15] A.E.W. Johnson, T.J. Pollard, L. Shen, Data Descriptor: MIMIC-III, a freely accessible critical care database, Sci. Data 35 (2016).

[16] Alian, A. A., & Shelley, K. H. (2014). Photoplethysmography [Journal Article]. Best practice & research. Clinical anaesthesiology, 28(4), 395-406. https://doi.org/ 10.1016/j. bpa. 2014. 08.006.

[17] Khawaja, R. A., Qureshi, R., Mansure, A. H., & Yahya, M. E. (2010). Validation of Datascope Accutorr Plus using British Hypertension Society (BHS) and Association for the Advancement of Medical Instrumentation (AAMI) protocol guidelines [Journal Article]. Journal of the Saudi Heart Association, 22(1), 1-5. https:// doi.org/10. 1016/j.jsha. 2010. 03. 001.